

The turbulent radial jet

By P. O. WITZE

Sandia Laboratories, Livermore, California

AND H. A. DWYER

Department of Mechanical Engineering, University of California, Davis

(Received 11 August 1975 and in revised form 29 January 1976)

A hot-film anemometer has been used to investigate the mean velocity and turbulence intensity distributions in turbulent radial jets. A geometric parameter termed the constraint ratio, defined as the ratio of nozzle diameter to separation distance, is shown to characterize radial-jet behaviour. Large values of the constraint ratio typify 'constrained' radial jets, for which the nozzle walls constrain the flow leaving the orifice to be parallel; a small constraint ratio is representative of two opposing free axisymmetric jets, the collision of which produces an 'impinged' radial jet. It is found that the well-behaved constrained radial jet spreads at the same rate as does the familiar plane jet, whereas the impinged radial jet spreads at a rate more than three times as fast. Neither type of radial jet is amenable to a self-similar analytic solution; however, while the impinged jet is shown to require numerical solution techniques, an empirical solution for the constrained jet is demonstrated.

1. Introduction

The radial jet, defined as the radially outward plane flux of fluid from a point source or a circular line source, has received little attention in the literature. This is somewhat surprising, since it represents a well-structured free turbulent shear flow of a fundamental nature. Radial jets also occur in practical applications such as ventilating ducts, internal combustion engine valves, and the analogous wall jet flows encountered in VTOL aircraft and turbine-blade cooling techniques.

Although a number of authors have studied various aspects of the radial jet, a comprehensive investigation has not been made. The earliest theoretical treatment of the problem appears to have been by Rumer (1949), who performed a mixing-length analysis analogous to Tollmein's (1926) plane-jet solution. Taliyev (1954) and Abramovich (1963) presented integral solutions derived from assumed velocity profiles. The analysis given by Squire (1955) is unique in that the complete Navier-Stokes equations are solved in spherical co-ordinates, rather than the usual boundary-layer approximations being assumed. Poreh & Cermak (1959) used an exchange-coefficient eddy-viscosity model to derive a solution comparable to Görtler's (1942) plane-jet results. More recently, Rodi (1972) has presented results of a numerical analysis that used a turbulent kinetic-energy/shear-stress model.

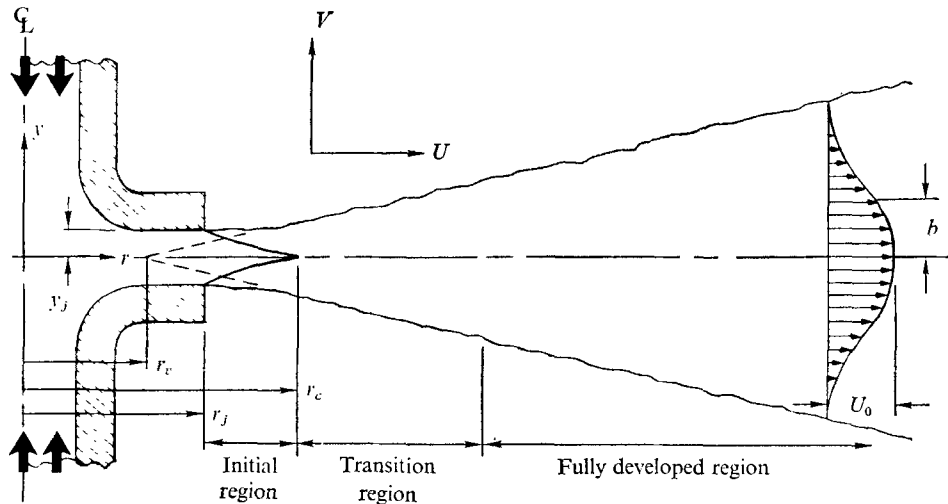


FIGURE 1. Characteristic structure of a constrained radial jet.

The earliest experimental investigation of the radial jet was by Tuve (1953), who measured the centre-line velocity and velocity profiles for two different radial-jet nozzle configurations, and also reported observations from smoke visualization studies. The most complete study to date has been that of Heskestad (1966), who used a hot-wire anemometer to measure both the mean velocity and turbulence quantities, including lateral distributions of the normal and Reynolds stresses, and the intermittency factor. However, only one radial-jet configuration was considered, for a single exit velocity.

The purpose of the present investigation was to characterize the general structure and behaviour of a broad range of radial-jet configurations. Indeed, it was found necessary to distinguish between two classes of radial jets as being either 'constrained' or 'impinged'. The constrained radial jet is the more conventional form and will be defined as the radially symmetric flow that results when fluid emerges from an annular orifice, such as the space between two parallel disks. The impinged radial jet is the planar, radially symmetric, free shear flow that results from the impingement of directly opposing circular jets of identical nozzle construction and balanced momentum fluxes. Measurements do not appear to have been reported for a turbulent impinged radial jet; Luna (1965) has performed a flow-visualization study of opposing free turbulent jets, which was carried out for the purpose of examining the stability of the resulting impinged radial jet. The only known measurements taken in two impinging turbulent jets are those of Kind & Suthanthiran (1973), who looked at the impinged plane jet that forms from the collision of two opposing plane wall jets.

2. Characteristic structure

The constrained radial jet is the axisymmetric counterpart of the more familiar plane jet. Unique to radial jets in general, however, is the appearance of a second geometric-similarity parameter. For the constrained radial jet depicted in figure 1,

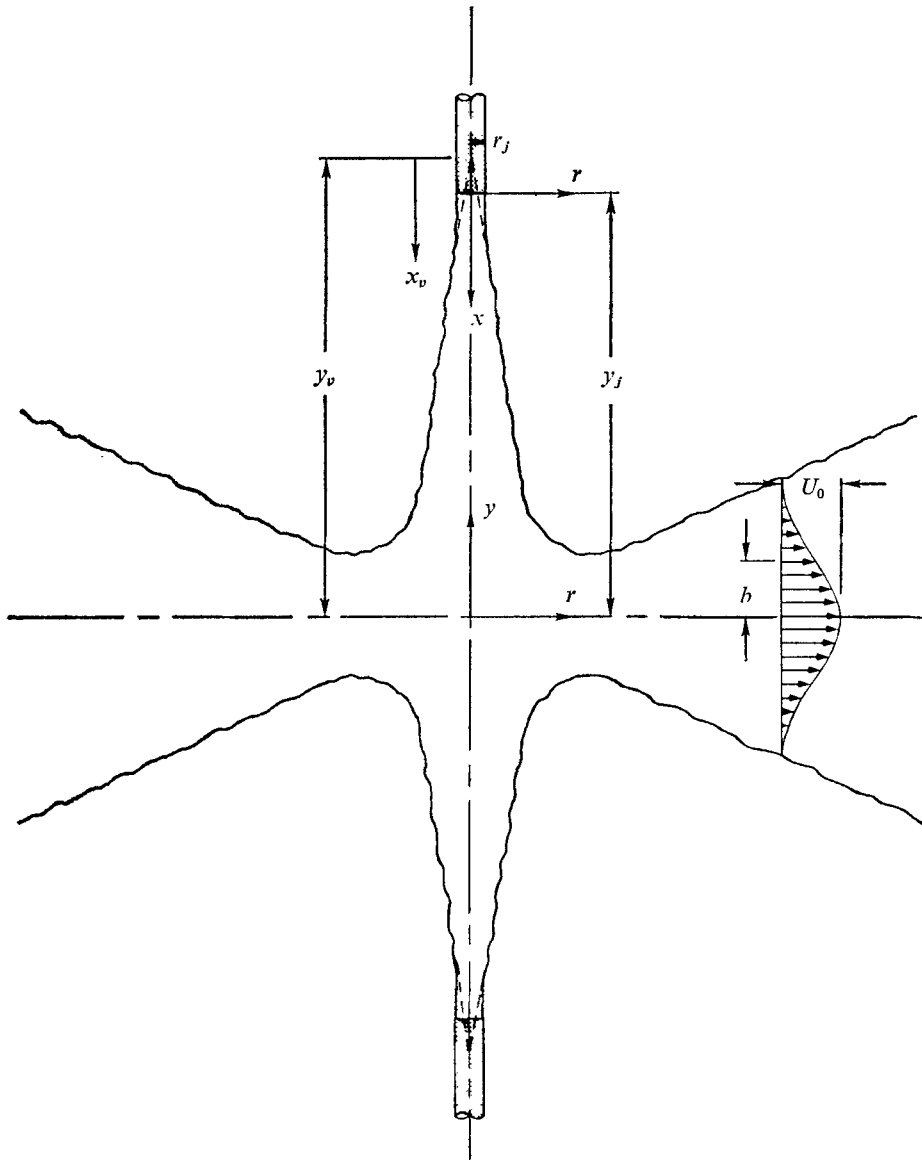


FIGURE 2. Characteristic structure of opposing free jets and the resulting impinged radial jet.

this additional dimension is the nozzle radius r_j , where the nozzle half-width y_j is analogous to the typical characteristic nozzle dimension of orifice size. The ratio of these geometric factors r_j/y_j will be termed the 'constraint ratio', since this quantity is indicative of the degree of constraint imposed on the jet flow by the nozzle walls. In the limit of an infinitely large radius, the constrained radial jet is equivalent to a plane jet.

The general flow structure of a constrained radial jet is similar to that of plane and axisymmetric free jets, except that the flow in the constant-velocity

inviscid core is not parallel, owing to the form of the continuity equation in cylindrical co-ordinates. The virtual origin of the fully developed region is located along a circle of radius r_v ; only for special conditions does it occur at the axis of symmetry, as a point source with $r_v = 0$.

As the constraint ratio is reduced by increasing the separation distance between nozzle sections, a point is reached beyond which the flow undergoes a change in structure such that, in the limit of very small constraint ratio, an impinged radial jet is achieved. This transition process is first indicated by a departure from well-behaved flow conditions at the nozzle orifice, in the form of increased turbulence intensities and non-parallel, non-uniform initial velocity profiles. Upon further separation of the nozzles, a situation is reached where the nozzle walls no longer influence the radial-jet structure. At this point the flow is characteristic of the impingement of the core regions of impinging axisymmetric jets from nozzles of arbitrary external geometry, such that the geometric-similarity parameter r_j must be redefined to be the internal radius of the nozzle. It is this impinging core-region flow that was observed by Luna (1965) to be unstable. A fully stable state is not regained until the separation distance exceeds two core lengths, which occurs at $r_j/y_j \cong 0.06$. It is at this point that a free impinged radial jet is formed.

Poreh & Cermak (1959) were the first to show that the similarity scale factor for an impinged radial jet is the distance y_0 from the impingement plane to the virtual origin of the free axisymmetric jet (see figure 2). This characteristic dimension might also be interpreted as indicating the maximum width of the shear layer of the impinging jets, since the width is known to grow linearly from the virtual origin. Additionally, it will be shown that the nozzle radius r_j and jet exit velocity U_j are also similarity parameters, since they characterize the total initial momentum flux of the flow field.

3. Theoretical solution

The approximate equations of motion for the radial jet are the time-averaged boundary-layer equations in cylindrical co-ordinates, for which the incompressible continuity and momentum equations are, respectively,

$$\partial(Ur)/\partial r + \partial(Vr)/\partial y = 0, \quad (1)$$

$$U \frac{\partial U}{\partial r} + V \frac{\partial U}{\partial y} = \frac{\partial}{\partial y} \left(\epsilon \frac{\partial U}{\partial y} \right). \quad (2)$$

Here U is the mean velocity in the main-flow, or radial direction r , whereas V is the lateral velocity component in the y direction; ϵ is the eddy diffusivity. It is important to notice that the U component of velocity occurs in two terms of the continuity equation, whereas for the more familiar axisymmetric jet it is the V component that occurs twice.

For the radial-jet equations to be self-similar, Rodi (1972) has shown that there are three similarity conditions to be satisfied: db/dr , $(b/U_0)dU_0/dr$, and b/r must all be constant, where U_0 is the centre-line mean velocity and b is the shear-layer half-width, defined as the point where $U = \frac{1}{2}U_0$. The first two criteria are

comparable to the conditions necessary for self-similar plane and axisymmetric jet solutions, and are satisfied when $b \sim r - r_v$ and $U_0 \sim (r - r_v)^{-1}$, where r_v is the radius of the virtual origin of the shear layer. The third criterion is unique to the radial jet, and requires that $r_v = 0$. Thus self-similar radial-jet equations can exist only for the special case where the virtual origin of the jet is located on the axis of symmetry, or in the limit where $r \gg r_v$. This is a significant result, since for a typical constrained radial jet $r_v \approx r_j$, although it will be shown that the singular occurrence of $r_v = 0$ can be achieved in the limit $r_j/y_j \rightarrow 0$, which is the case of the impinged radial jet. The condition that $r_v = 0$ is therefore a necessary condition for the occurrence of what will be called an 'ideal' radial jet, implying that the jet is both well behaved and analytically self-similar.

The fact that the constrained radial jet is not a self-similar flow precludes the possibility of a purely analytic solution. However, experimental results to be presented below do provide the necessary information for an empirical analysis. First, it is found that the radial-jet half-width does grow linearly from the virtual origin, such that

$$b = m(r - r_v), \quad (3)$$

where $m = db/dr$ is the spreading rate. Second, it will be shown that the velocity profiles across the shear layer have a self-similar form that can be expressed as

$$U/U_0 = \operatorname{sech}^2(0.881y/b), \quad (4)$$

which is the velocity profile derived by Poreh & Cermak (1959) using Prandtl's constant-exchange-coefficient model for the eddy diffusivity. For conservation of total momentum it follows that

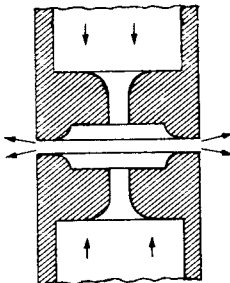
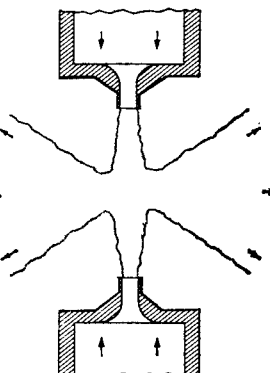
$$\frac{U_0}{U_j} = \left(\frac{1.32r_j y_j}{mr(r - r_v)} \right)^{\frac{1}{2}}, \quad (5)$$

for which there are two empirical quantities to be determined, m and r_v . However, it will be shown that, for well-designed nozzles producing constrained radial jets where the exit velocity from the orifice is parallel, m is a universal constant having the value 0.106; and for large values of r/y_j , $r_v \approx r_j$. Unfortunately, it will also be shown that an analytic solution cannot exist for the impinged radial jet.

4. Experimental results

The experimental programme was formulated with the intent of including as comprehensive a range of independent parameters as was reasonably possible. The resultant matrix of experimental conditions is summarized in table 1. Shown also are schematic diagrams of the basic nozzle configurations used.

One of the experimental difficulties encountered was the occurrence of a significant boundary layer on the inner walls of the jet nozzles. Since this manifests itself as a net mass and momentum deficit of the jet flow, techniques had to be developed to correct for the wall boundary-layer effect. The correction takes the form of an 'effective' nozzle width, calculated from a momentum balance between the real non-uniform initial velocity profile and an ideal uniform profile across the effective nozzle width. For further details, see Witze (1974).

Constrained radial jet	U_j (m s ⁻¹)	r_j (cm)	r_v (cm)	y_j (cm)†	Symbol
	60.7	1.59	‡	0.0186	⊠
	30.5	1.59	1.46	0.02§	⊠
	30.8	1.59	1.52	0.0414	⊠
	30.2	1.59	1.57	0.0665	△
	29.6	1.59	1.58	0.0919	◇
	30.5	3.18	3.15	0.0148*	⊠
	26.8	3.18	2.97	0.0363	⊠
Impinged radial jet	U_j (m s ⁻¹)	r_j (cm)†	y_v (cm)	y_j (cm)	Symbol
	30.8	0.30	13.3	12.7	⊠
	30.5	0.30	10.2	9.53	⊠
	30.5	0.30	6.99	6.35	⊠
	61.3	0.30	13.3	12.7	⊠
	30.8	0.43	9.86	8.97	◇

† Corrected for nozzle-wall boundary-layer effects.

‡ Not measured. Assumed to be 1.46 cm.

§ Empirically selected because of non-analytic nozzle-wall boundary layer.

* Fully developed channel flow.

TABLE 1. Summary of experimental conditions

The jets were formed by commercial-grade dry air supplied from standard compressed-gas bottles. A laser beam was used to align the nozzles producing impinged radial jets. The mean velocity measurements were taken with a linearized constant-temperature anemometer. The linearizer output was digitized and processed with an on-line PDP-8 mini-computer. A single-sensor, hot-film probe was used throughout, oriented normal to the main-flow direction. This choice excluded the possibility of determining the lateral velocity component, which for impinged radial jets was found to be significantly large. However, because the relative turbulence intensity was also large, it is believed that the added sensitivity that an inclined sensor would have to the third fluctuating velocity component would seriously impair the accuracy of two-component measurements.

For a major portion of the shear flows studied, relative turbulence intensities were found to be in excess of 20%, at which point the nonlinear response of the anemometer to large directional fluctuations in velocity produces a systematic error. Additionally, when the turbulence intensity exceeds about 30%, there is

a finite probability of a reversal in flow direction; this condition cannot be detected by the probe, and thus another systematic error results. While it is admittedly not possible to make accurate corrections for these conditions when the turbulence becomes too high, some improvement can be achieved by applying the correction proposed by Corrsin (1943):

$$U = \frac{U_{\text{meas}}}{1 + 0.25(u/U)^2}, \quad (6)$$

where, in deference to the usually applied assumption of isotropic turbulence, it has been assumed that $\overline{v^2} \approx \overline{w^2} \approx \frac{1}{2}\overline{u^2}$ on the basis of experimental results of Heskestad (1966) (u , v and w are the orthogonal components of the turbulent velocity fluctuations). It is believed that this correction provides quantitatively accurate data for turbulence intensities less than 30 %, while for greater levels the data might better be described as being qualitatively representative of the actual flow. The corresponding error in the measurement of the turbulent fluctuation u was shown by Parthasarathy & Tritton (1963) to be small for a linearized anemometer; thus no correction need be applied for u .

4.1. Lateral profile data

Mean velocity profile data for a typical nozzle configuration producing a constrained radial jet are shown in figure 3, compared with the self-similar velocity profile given by (4). While the measured values are clearly self-similar, it is also evident that the theory underpredicts the data by a considerable amount in the outer region. The apparent asymptotic trend of the data towards a non-zero edge velocity suggests that a measurable lateral velocity component may be present. This is a reasonable conclusion, since the orientation of the hot-film probe was such that the sensor was perpendicular to the r, y plane and thus responded to the total velocity vector $U_{\text{meas}} = (U^2 + V^2)^{\frac{1}{2}}$. By introducing the velocity profile represented by (4) into the continuity equation and using a spreading rate $m = 0.106$ (shown in the next section to be representative of a well-behaved constrained radial jet), it can be shown that, in the limit as $y/b \rightarrow \infty$, $V/U_0 \rightarrow -0.12$, which is very close to the magnitude of the asymptotic value indicated in figure 3.

Mean velocity profile data for a typical impinged radial jet are shown in figure 4, compared with the self-similar profile. Again, it is seen that the profiles are of a self-similar form, although there is considerably more scatter in the data than in the constrained-jet case. Additionally, owing to the higher entrainment rate of the impinged jet, the disagreement between data and theory at the outer edge due to the lateral velocity component is even more pronounced.

The turbulence intensity data corresponding to the mean velocity profile data just presented are given in figures 5 and 6, where $u' \equiv (\overline{u^2})^{\frac{1}{2}}$. The data along the centre-line at $y/b = 0$ indicate that self-preservation of the turbulence intensities was not achieved, since u'_0/U_0 is not constant. The 60–70 % intensity levels shown are much higher than can be accurately measured with a hot film. However, the excellent consistency of the mean velocity data suggests that the results shown are accurate enough to be meaningful.

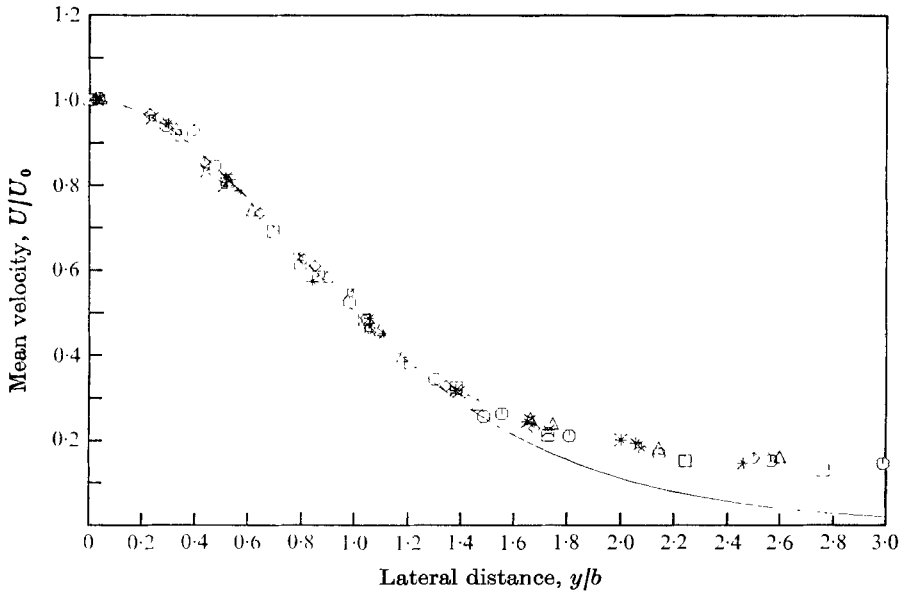


FIGURE 3. Mean velocity profiles for constrained radial jet for $U_j = 30.2 \text{ m s}^{-1}$, $r_j = 1.59 \text{ cm}$, $y_j = 0.0665 \text{ cm}$. $(r-r_0)/y_j$: \square , 38.3; \circ , 76.5; \triangle , 115; \diamond , 153; \boxtimes , 191; \ast , 229. —, equation (4).

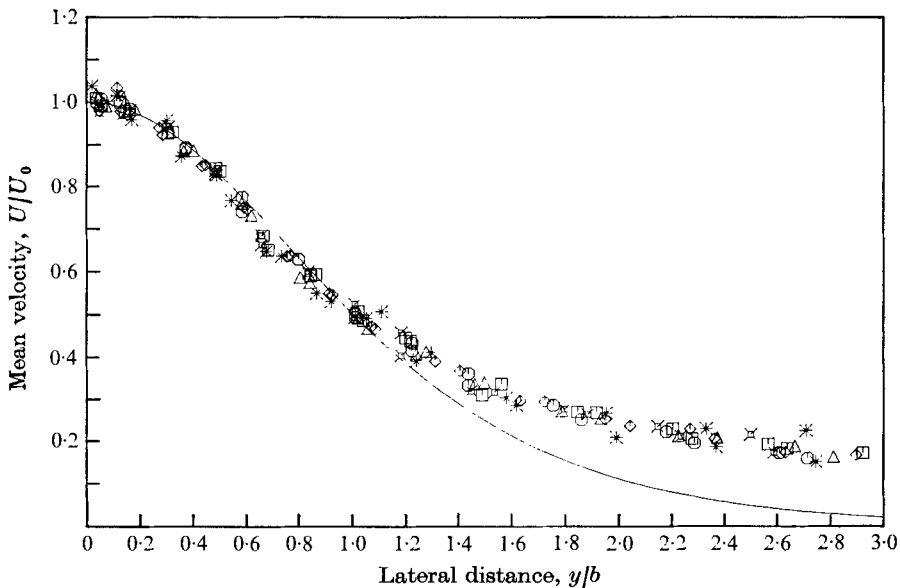


FIGURE 4. Mean velocity profiles for impinged radial jet for $U_j = 30.8 \text{ m s}^{-1}$, $r_j = 0.30 \text{ cm}$, $y_j = 6.35 \text{ cm}$. r/y_j : \square , 0.2; \circ , 0.4; \triangle , 0.6; \diamond , 0.8; \boxtimes , 1.0; \ast , 1.2. —, equation (4).

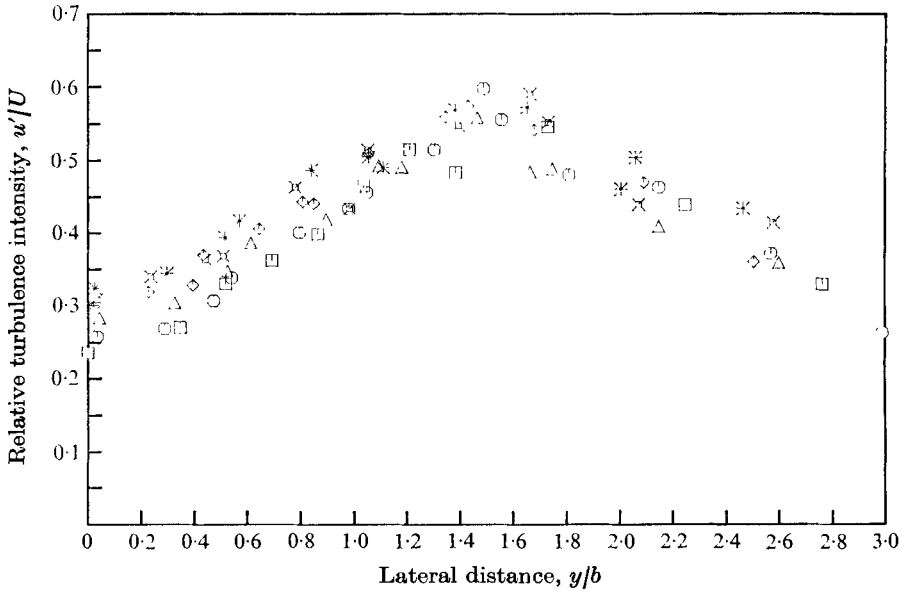


FIGURE 5. Relative turbulence intensity profiles for constrained radial jet. Conditions and symbols as for figure 3.

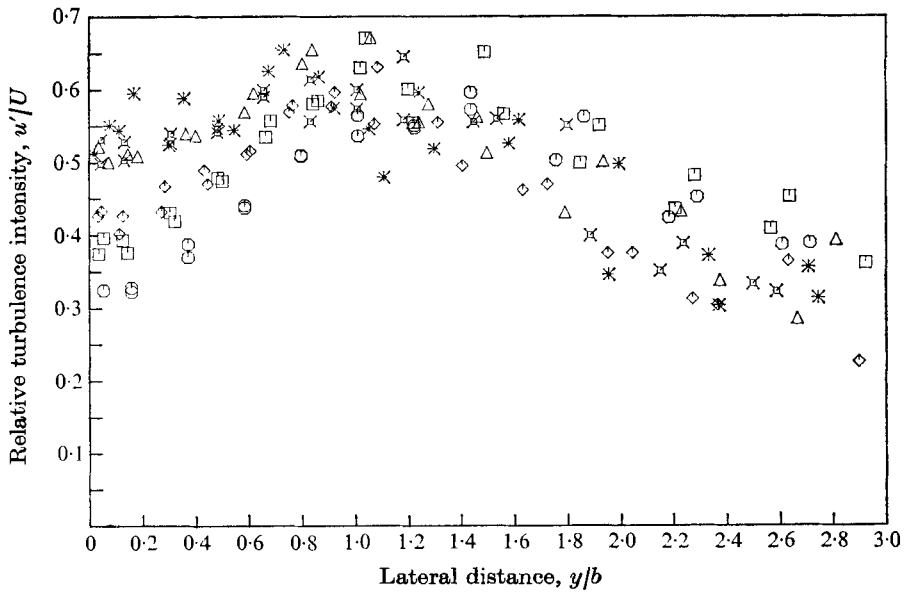


FIGURE 6. Relative turbulence intensity profiles for impinging radial jet. Conditions and symbols as for figure 4.

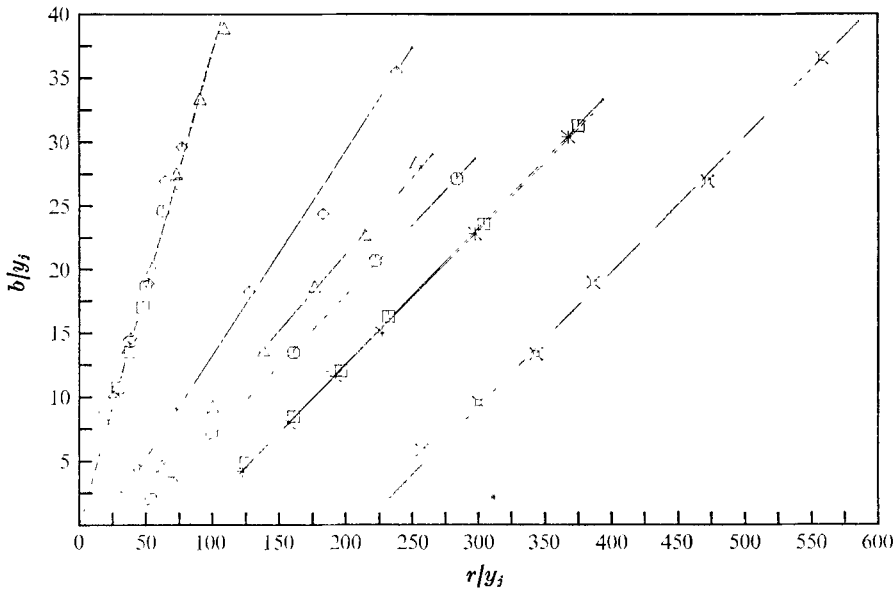


FIGURE 7. Radial-jet half-widths for different nozzle configurations. Symbols as given in table 1. —, constrained radial jet, equation (3); ---, impinging radial jet, $b = 0.37r$, $(r/y_j) \times 100$, $(b/y_j) \times 100$.

4.2. Half-width, virtual origin and centre-line turbulence measurements

It is conventional practice to establish the existence of self-similarity from velocity profile data such as were given in figures 3 and 4. However, this can be misleading since the data have been forced to pass through specific points on the axis and at the half-width. Perhaps a more certain indicator of self-similarity is the linearity of the jet half-width, shown in figure 7 as determined from the profile measurements. The origin of each of the curves shown is approximately at the nozzle radius, such that the value of the abscissa at the origin is representative of the constraint ratio. Thus it is seen that a constant spreading rate exists for large constraint ratios, whereas, if the constraint ratio is reduced, the spreading rate increases until the impinging-radial-jet limit is reached.

The spreading rates and virtual-origin locations determined from figure 7 are shown plotted versus the constraint ratio in figure 8. For $r_j/y_j > 40$ the spreading rate is approximately constant, with an asymptotic value of 0.106, which in the limit $r_j/y_j \rightarrow \infty$ represents the plane jet. This is very close to the observations by Newman (1967), who determined an average value for the plane jet of 0.104, based on a comprehensive review of the experimental literature up to 1965.

As the constraint ratio is reduced to zero, it is seen that the spreading rate suddenly increases to a maximum value of 0.37 for the impinging radial jet. It is important to stress, however, that the shape of the spreading-rate curve between the impinging-radial-jet and plane-jet limits is not universal, but rather is dependent on the internal geometry of the radial-jet nozzles. Similarly, the virtual-origin-location curve shown in figure 8 is not universal, except for the limiting-case end points. For constrained radial jets, the virtual origin was always found

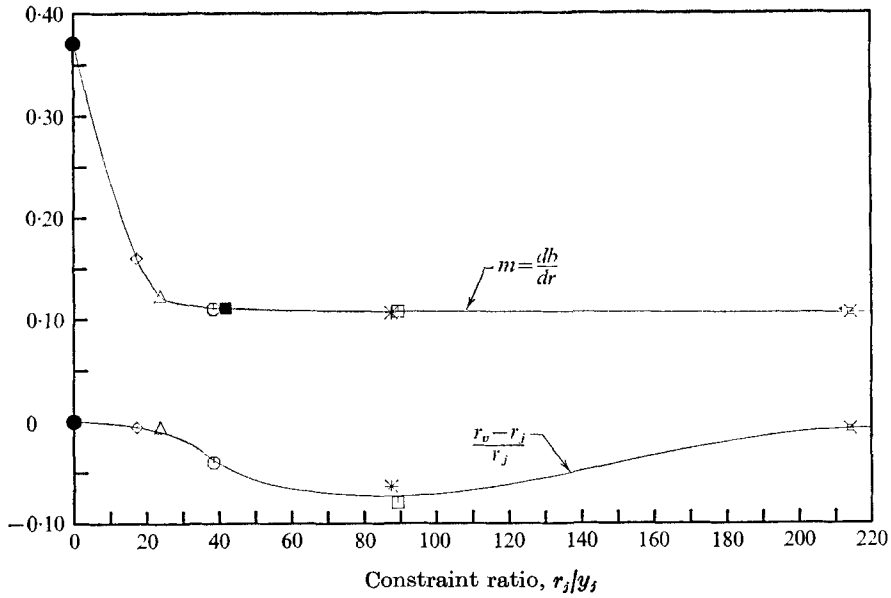


FIGURE 8. Dependence of radial-jet spreading rate and virtual-origin location on the constraint ratio. Symbols for constrained radial jet as given in table 1; ●, impinging radial jet; ■, Heskestad (1966).

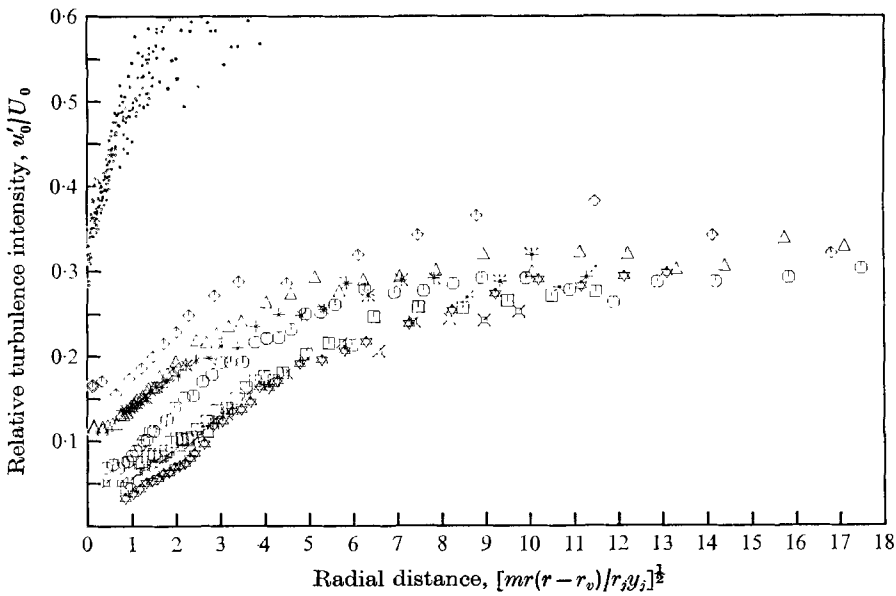


FIGURE 9. Radial-jet relative turbulence intensities along the centre-line. Constrained-jet symbols as given in table 1; ○, impinging radial jet.

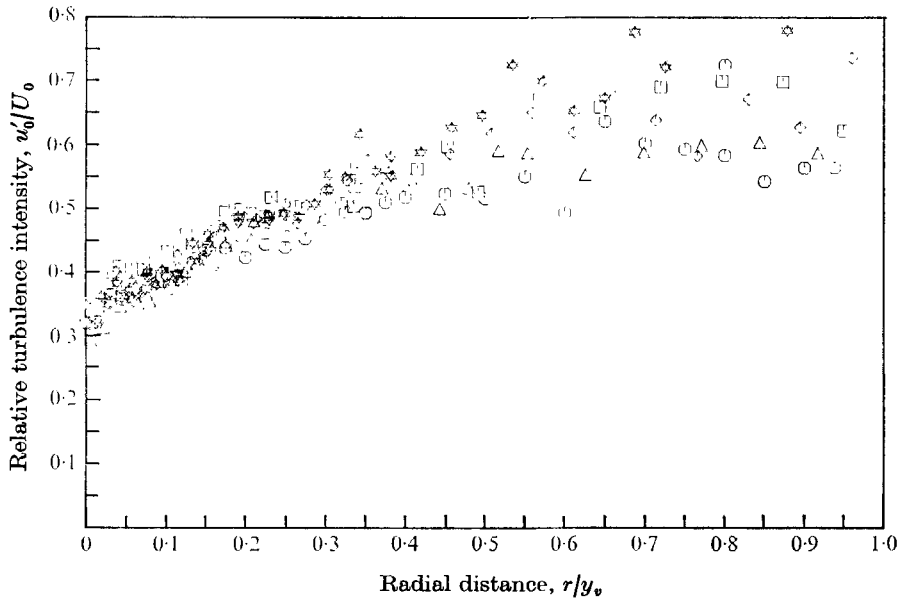


FIGURE 10. Relative turbulence intensities for impinged radial jet along the centre-line. Symbols as given in table 1.

to lie inside the nozzle, but never by more than about 8% of the nozzle radius. This supports the approximation that at distances far from the orifice of a constrained radial jet $r_v \approx r_j$.

The large increase in jet spreading rate at small values of the constraint ratio is accompanied by a similarly large increase in the relative turbulence intensity at the jet origin, as shown in figure 9. However, it is not the increased turbulence that is enhancing the spreading rate. This is illustrated by the case where $U_j = 26.8 \text{ m s}^{-1}$, which had a very high initial turbulence level, and yet was shown in figure 8 ($r_j/y_j = 87.4$) to have a well-behaved spreading rate. Indeed, it is generally accepted that initial turbulence intensity levels at a jet's source do not influence the final self-preserving form of the shear layer, other than in the location of the virtual origin. This is indicated by the asymptotic behaviour of the relative intensity data presented in figure 9, which are seen to converge to a value of approximately 32%, irrespective of the initial turbulence levels.

Because the spreading rate does correlate with the nozzle constraint ratio, but not with the initial turbulence level, it can be concluded that the non-parallel nature of the initial jet conditions must be the property characterizing non-ideal radial-jet behaviour. This hypothesis is consistent with the observed universal spreading rate of impinged radial jets, since it can be argued that colliding self-similar axisymmetric jets will produce self-similar radial-jet initial conditions that are both non-parallel and independent of the separation distance. Thus it is only when constraining nozzle walls are introduced that the self-similar initial conditions of impinging jets become altered, to the point that in the limit of large constraint ratios the initial flow becomes parallel, and a well-behaved constrained radial jet results.

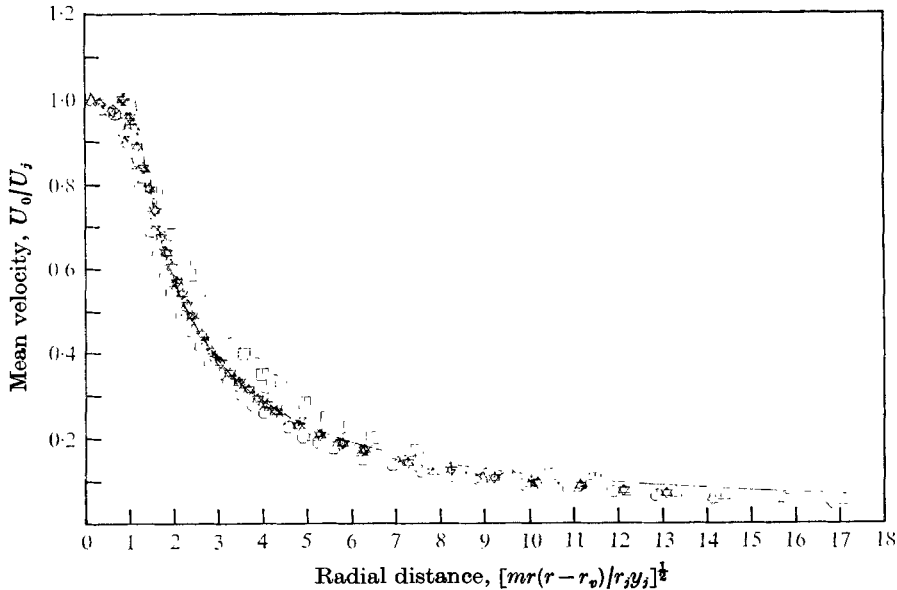


FIGURE 11. Mean velocities for constrained radial jet along the centre-line. Symbols as given in table 1. —, equation (5).

The centre-line turbulence intensity data for impinged radial jets are shown again in greater detail in figure 10. It is evident that in the vicinity of the stagnation point the data behave in a nearly self-similar fashion. The small variation in intensity does correlate with the separation distance, suggesting that the initial scale of the turbulence is related to the width of the impinging jets at the point of collision, as one might expect. It is also apparent from this figure that at distances far from the stagnation point the flow is not self-similar, a point that will be discussed in greater detail below. (It should be mentioned that two significant experimental limitations present themselves in figure 10. First, the mean velocity at the stagnation point should obviously be zero, resulting in an undefined relative intensity. However, owing to directional ambiguity the anemometer interprets the turbulence at the stagnation point as being a mean velocity. Second, with the hot-film sensor aligned parallel to the opposing jets' centre-line, the turbulence intensity measured at the stagnation point is in error by $\sqrt{2}$, since the probe is equally sensitive to both the u and the v component of the turbulence. Because this error drops off in an unknown fashion as the probe is moved radially outwards into a region of large mean velocity, it is not practical to attempt a correction.)

4.3. Centre-line velocity data

Experimental measurements of centre-line velocities in constrained radial jets are shown in figure 11. The similarity parameter used along the abscissa includes two empirically determined quantities, these being the spreading rate and virtual-origin location. The values used were taken from figure 8. The theoretical

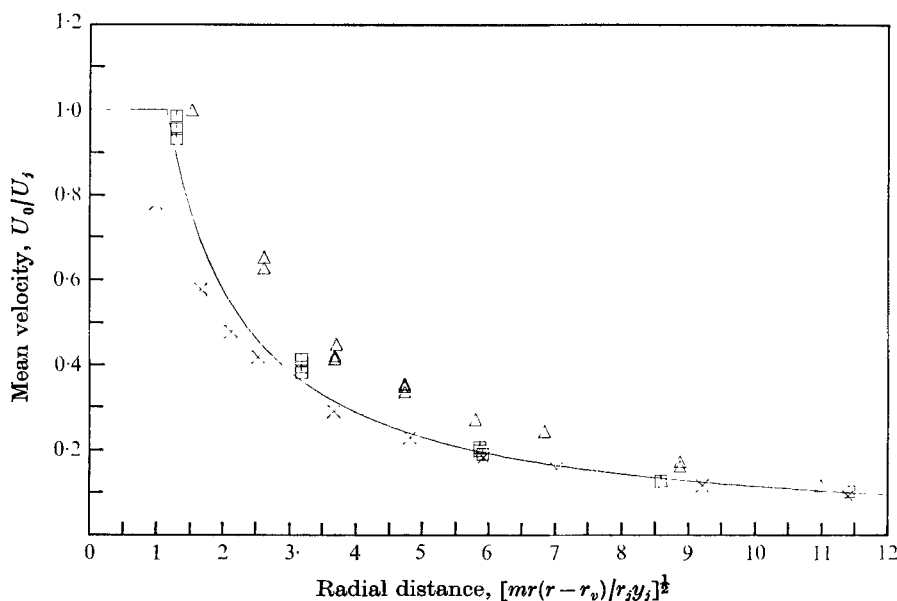


FIGURE 12. Mean velocities for constrained radial jet along the centre-line. Heskestad (1966): \times , $U_j = 46.3 \text{ m s}^{-1}$, $r_j = 15.2 \text{ cm}$, $y_j = 0.366 \text{ cm}$. Tuve (1953): \square , $U_j = 37.2\text{--}79.2 \text{ m s}^{-1}$, $r_j = 2.54 \text{ cm}$, $y_j = 0.318 \text{ cm}$; \triangle , $U_j = 5.49\text{--}11.2 \text{ m s}^{-1}$, $r_j = 17.8 \text{ cm}$, $y_j = 1.27 \text{ cm}$.

curve shown in the figure was computed using (5), where the core length is found from the condition that $U_0/U_j = 1$, giving

$$r_c = \frac{1}{2}[r_v + (r_v^2 + 5.288r_j y_j/m)^{1/2}]. \quad (7)$$

Agreement between data and theory is reasonably good, although in general the prediction is high. Within the initial region, this type of disparity is characteristic of most free-jet analyses owing to the idealized modelling of the jet core. However, the overprediction of theory at large distances from the source is more fundamental in nature, and is believed to be due to the assumptions inherent in working with the boundary-layer form of the momentum equations. For example, for the well-behaved constrained radial jet, the spreading rate for the point where $U/U_0 = 0.01$ is $y/r = 0.36$ by using (4). This does not correspond to a 'very thin' shear layer, for which the necessary condition is that $y/r \ll 1$.

Shown in figure 12 are the centre-line velocity data reported by Tuve (1953) and Heskestad (1966). Agreement of the latter with theory is very good at large distances from the orifice, but appears to be quite low in the initial region. This can probably be attributed to the unresolved disparity of an observed virtual origin for the velocity data that was measurably smaller than that found for the half-width. (In preparation of Heskestad's data for this figure, it was deemed more consistent to use his measured values for m and r_v , with the virtual origin being that which corresponded to the half-width data. Additionally, the liberty has been taken of applying the same nozzle boundary-layer correction to Heskestad's data as was used for the current measurements (see Witze 1974).) For

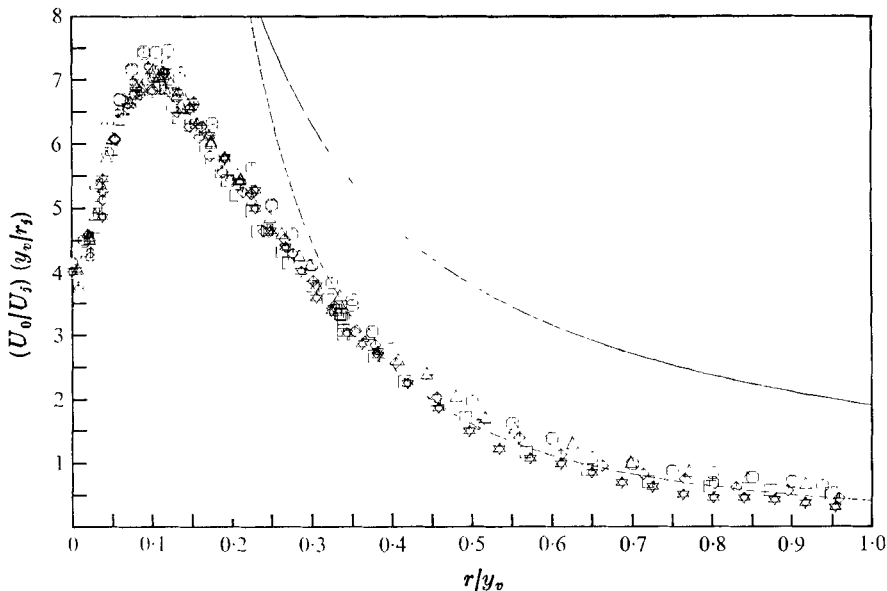


FIGURE 13. Mean velocities for impinged radial jet along the centre-line. Symbols as given in table 1. —, equation (8); ---, equation (9).

the measurements by Tuve shown in the same figure, it was necessary to assume values of $m = 0.106$ and $r_v = r_j$, since these quantities were not reported. Good agreement with theory was found for the smaller nozzle, which had a contoured contraction in the orifice approach section. On the other hand, agreement with the data for the larger nozzle is very poor. This result can be attributed to the nozzle design, which consisted of a sharp-edged sheetmetal supply duct opposed by a dead-end duct. Thus the nozzle was not symmetric about the impingement plane, and the vena-contracta of the sharp edge could be expected to place r_v outside the duct radius, which would explain at least part of the observed discrepancy between data and theory. (Tuve's centre-line velocity data do include a discharge-coefficient correction, although specifics of its evaluation are not known.)

Mean velocity measurements taken along the impinged radial jet's centre-line are shown in figure 13. While experimental-facility limitations did not permit a complete traverse of the flow field on either side of the stagnation point, enough data could be taken to assure symmetry of the flow across the impingement zone. The measured velocity in the stagnation region is known to be in error, as the stagnation-point velocity should be zero. The form of the similarity parameters is significant in that they are characteristic of the free-axisymmetric-jet conditions at the point of impact. That is, the centre-line velocity of an axisymmetric jet decays inversely with the dimensionless distance x_0/r_j , as the jet spreads linearly with the total distance x_0 .

It has been shown that two of the requirements for self-similarity are satisfied by the impinged radial jet; namely, that the shear layer should grow linearly from a virtual origin located at $r = 0$. The remaining condition is that the centre-

line velocity should decay inversely with radial distance, which is a result of the condition that radial momentum be conserved. If it is assumed that the impinging radial jet's total radial momentum is equal to the sum of the momentum fluxes from the opposing axisymmetric nozzles, it can be shown that

$$\left(\frac{U_0}{U_j}\right)\left(\frac{y_v}{r_j}\right) = 1.89\left(\frac{y_v}{r}\right), \quad (8)$$

where (4) has been used for the velocity profile, with $m = 0.37$. This result is shown compared with centre-line velocity data in figure 13. It is evident that (8) severely overpredicts the momentum in the flow. This discrepancy is due to more than just the assumed level of total momentum, however, since a nonlinear least-squares fit to the data results in

$$\left(\frac{U_0}{U_j}\right)\left(\frac{y_v}{r_j}\right) = 0.4\left(\frac{y_v}{r}\right)^2, \quad (9)$$

which indicates that the actual rate of centre-line velocity decay is far greater than that predicted by the momentum conservation equation.

The source of this 'momentum loss' is believed to be failure to satisfy the assumed condition of parallel flow. This non-parallel behaviour was clearly indicated by figure 4, where it is evident that a measurable lateral velocity component is present. Such a large lateral component violates the approximations inherent in the boundary-layer form of the governing equations used to model the flow. Indeed, a complete reassessment of the full Navier-Stokes equations is necessary, since additional terms corresponding to the high turbulence levels may also need to be retained.

In closing, it is apparent that the large lateral velocity component and the extremely high turbulence levels encountered in the impinging radial jet exceed both the experimental and the analytic capabilities employed. Inclusion of the higher-order terms in the momentum equations will require a numerical solution of the full elliptic form of the Navier-Stokes equations, a task that will be severely hampered by the absence of prescribed boundary conditions.

REFERENCES

- ABRAMOVICH, G. N. 1963 *The Theory of Turbulent Jets*. MIT Press.
- CORRSIN, S. 1943 Investigation of flow in an axially symmetrical heated jet of air. *N.A.C.A. Wartime Rep. W-94*.
- GÖRTLER, H. 1942 Berechnung von Aufgaben der freien Turbulenz auf Grund eines neuen Näherungsansatzes. *Z. angew. Math. Mech.* **22**, 244-254.
- HESKESTAD, G. 1966 Hot-wire measurements in a radial turbulent jet. *J. Appl. Mech.* **88**, 417-424.
- KIND, R. J. & SUTHANTHIRAN, K. 1973 The interaction of two opposing plane turbulent wall jets. *J. Fluid Mech.* **58**, 389-402.
- LUNA, R. E. 1965 A study of impinging axisymmetric jets and their application to size classification of small particles. Ph.D. dissertation, Princeton University.
- NEWMAN, B. G. 1967 Turbulent jets and wakes in a pressure gradient. In *Fluid Mechanics of Internal Flow*, pp. 170-209. Elsevier.

- PARTHASARATHY, S. P. & TRITTON, D. J. 1963 Impossibility of linearizing a hot-wire anemometer for measurements in turbulent flows. *A.I.A.A. J.* **1**, 1210–1211.
- POREH, M. & CERMAK, J. E. 1959 Flow characteristics of a circular submerged jet impinging normally on a smooth boundary. *6th Midwestern Conf. Fluid Mech., University of Texas, Austin*, pp. 198–212.
- RODI, W. 1972 The prediction of free turbulent boundary layers by use of a two-equation-model of turbulence. Ph.D. dissertation, University of London.
- RUMER, YU. B. 1949 Turbulent source of free annular jet. *Dokl. Akad. Nauk S.S.S.R.* **64**, 463–466.
- SQUIRE, H. B. 1955 Radial jets. *50 Jahre Grenzschichtforschung*, pp. 47–54. F. Vieweg & Son.
- TALIYEV, V. N. 1954 Fundamental principles governing an annular turbulent source. *Dokl. Akad. Nauk S.S.S.R.* **94**, 405–408.
- TOLLMEIN, W. 1926 Calculation of turbulent expansion processes. *Z. angew. Math. Mech.* **6**, 468–478.
- TUVE, G. L. 1953 Air velocities in ventilating jets. *Heat. Pip. Air Cond.* **25**, 181–192.
- WITZE, P. O. 1974 A study of impinging axisymmetric turbulent flows: the wall jet, the radial jet, and opposing free jets. Ph.D. dissertation, University of California, Davis.